Two separate but interconnected pattern formation systems are required to control body-axis and head-organiser formation in *Hydra*

Moritz Mercker[1*], Anja Tursch[2], Frits Veerman[3], Alexey Kazarnikov[1], Stefanie Höger[2], Tobias Lengfeld[2], Suat Özbek [2], Thomas W Holstein[2], and Anna Marciniak-Czochra[1]

[1] Institute of Mathematics, Heidelberg University, Heidelberg, Germany
[2] Department of Molecular Evolution and Genomics, Centre for Organismal Studies (COS), Heidelberg University, Heidelberg, Germany
[3] University of Leiden, Mathematical Institute, Leiden, The Netherlands

[*] Corresponding author. E-mail: mmercker_bioscience@gmx.de

ABSTRACT

Formation of the body axes and the apical termini are fundamental steps during animal development. Here, nuclear β-catenin and canonical Wnt3 have been identified as major players in *Hydra*, which belongs to the early diverging phylum of cnidaria. However, both molecules have previously been assumed to be part of the same pattern formation system. In this study, we revised this view by combining mathematical modeling with previous and new experimental data demonstrating that they contribute to two largely independent *de novo* pattern formation systems in *Hydra*. Notably, β-catenin (possibly in interplay with other Wnts) appeared to act at the whole-body scale contributing to axis formation, whereas Wnt3 was involved in a downstream pathway driving small-scale patterning of the head. These results also suggest that these mechanisms may be more complex in other animals, in which axis and head formation have previously been attributed to a single pattern formation mechanism.

Keywords: Pattern formation, *Hydra*, Wnt signaling, Wnt3, β-catenin, mathematical modeling, reaction-diffusion equations, axis formation, head organiser, self-organization

INTRODUCTION

Understanding the mechanisms responsible for formation of the primary body axis is a crucial issue in developmental biology (65). The process can be based on maternally derived pre-patterns, such as in the fruit fly embryo (17), or axis formation during embryogenesis can be a self-organized process, as demonstrated in various developmental systems ranging from simple metazoans to complex mammalian organs (26; 63; 72; 85; 94). Moreover, even in vertebrate systems, recent data have revealed that spontaneous symmetry-breaking occurs in the absence of extra-embryonic tissues (4; 83; 86). Consequently, self-organization may serve as a mechanism to ensure the robustness of developed structures under various intrinsic and extrinsic conditions.

Cnidarians provide a popular model system for studying general and transmissible developmental principles (21; 37; 42), and the freshwater polyp *Hydra* has been used to study development and regeneration for nearly 300 years. *Hydra* is used to systematically investigate axis and head formation under different natural and perturbed conditions. Head and axis patterning are constitutively active in adult polyps, to ensure maintenance of the body axis amidst a continuous flow of self-renewing and differentiating cells (7; 8; 9). Moreover, the system regenerates ”extremities”, such as the head and foot, as shown by Trembley in 1740 (82) and subsequently demonstrated in a range of tissue manipulation experiments (6; 60). Notably, *Hydra* can also regenerate entire polyps from dissociated and re-aggregated cells (26), providing a paradigm for *de novo* pattern formation (70; 79). Furthermore, *Hydra* tissue pieces can be transplanted from a donor to a host polyp by ”grafting”, thus providing a model for mutual spatial interactions between tissue pieces from different body regions and different morphogenetic backgrounds (16; 47; 48; 73; 97). Body-axis and head formation also occur during budding, representing *Hydra*'s asexual form of reproduction, where buds evaginate and grow in the budding region of the mother polyp, eventually detaching as functional polyps (64). Finally, because *Hydra* also undergoes sexual reproduction, the mechanisms driving axis and head formation during embryogenesis can also be studied (19; 24; 50).

The mechanisms controling the formation, regeneration, and maintenance of the body axis, including the head, remain an important issue in *Hydra* research (20; 28; 77; 91). Early grafting and regeneration experiments suggested the existence of so-called positional information, which informed cells about their relative position along the body axis, thus determining their functions (16; 26; 47; 48; 82). Recent studies identified several candidate molecules involved in these processes, including nuclear β-catenin (hereafter β-catenin) and HyWnt3 (hereafter Wnt3). These were identified as key players in head and axis formation in *Hydra* (15; 23; 35; 78), suggesting that canonical Wnt signaling is the force driving the patterning process. Canonical Wnt signaling has also been studied intensively in a range of model organisms, and Wnt activity, linked to translocation of β-catenin into the nucleus, was shown to be involved in the control of various developmental processes (reviewed in (3; 41)). These findings led to the conclusion that the canonical Wnt signaling pathway constituted the core structure of the patterning system in *Hydra*, further suggesting that Wnt3 and β-catenin were involved in the same pattern formation system, with no distinction between the mechanisms regulating the processes of body-axis and head patterning (37; 51; 67). However, recent studies have proposed independent regulation of Wnt3 by inhibitors at the transcriptional or posttranslational level, such as Sp5 (90) or HAS-7 (99), acting in addition to the main β-catenin patterning mechanism. Nevertheless, it remains unclear how these two regulatory mechanisms work together in the context of pattern formation: is there an overall single body-axis patterning system in which Wnt3-induced head formation is based on thresholds (resembling Wolpert's seminal theory of positional information (96)), or are there two interconnected but autonomous pattern formation systems for the head and for body-axis formation?

We propose to approach this question using mathematical models and model-based analyses of experimental data. *Hydra*

has attracted extensive attention in theoretical pattern formation research, including the seminal paper by Alan Turing (84), who proposed that specific nonlinear interactions facilitated by different diffusivities may explain the *de novo* emergence of patterns, similar to *Hydra* regeneration following cutting experiments. The most famous realisation of Turing's idea in a mathematical model of biological pattern formation was the activator–inhibitor model proposed by Alfred Gierer and Hans Meinhardt (25; 27; 51; 52; 54). That abstract model provided hints as to how cell-to-cell communication through interacting diffusive molecules may lead to symmetry breaking and emergence of spatially heterogeneous patterns. In recent years, alternative models to the activator-inhibitor model have been proposed, e.g. models based on the coupling of diffusive and non-diffusive components of the system, such as cell-localized non-linear feedback (49; 57) or mechanical signal transduction (56; 58). However, so far all models discussed in the context of pattern formation in *Hydra* were based on the assumption that both axis and head formation are driven by a single control loop with canonical Wnt signaling as its core structure (52; 53). As noted above, this hypothesis was in agreement with the results of several *Hydra* experiments demonstrating that both nuclear β-catenin and Wnt3 exhibited spatio-temporal correlations: e.g., expression levels of both were highest at the oral end of the *Hydra* body column and at the tips of developing buds (7; 8; 14; 23; 35; 37; 43). Furthermore, pharmaceutical or transgenic induction of nuclear β-catenin induced a transient increase of *Wnt3*-ranscript in the body column, which was otherwise absent (15; 23; 29; 30), and several studies also showed that *Wnt3* expression depended on β-catenin (62; 67; 90). However, previous experiments also revealed that, although there was a general mutually positive relationship between β-catenin and Wnt3, both molecules showed differences with respect to their regulation in space and time, and with respect to their putative functions. Although recent studies have suggested a more nuanced view (90; 99), a rigorous analysis of the regulation of these molecules is still lacking.

In the current study, we combine a model-based analysis with a review of previous and new experimental data, suggesting the existence of two distinct and autonomous patterning systems governing body axis and head formation, respectively. Simulations of a model integrating β-catenin and Wnt3 into a single patterning mechanism, following the late Meinhardt model (52; 53), point to various experiments that cannot be explained by a single pattern formation scheme, and require a model that separates the two systems working on different scales. This includes several experiments in which organiser-specific genes were transiently or permanently expressed in multiple closely spaced spots. In contrast, in systems based on a single body-axis pattern formation mechanism, the distance between organisers is similar to the scale of the body axis, which contradicts experimental observations. In addition, supported by model analysis, we demonstrate that the development of multiple heads as a result of overexpression of putative activator candidates (such as *Wnt3*) cannot be explained by a single pattern formation loop, such as the activator–inhibitor scheme or related models.

This apparent discrepancy between the model and experiments prompt us to extend the existing models to describe the dynamics of nuclear β-catenin and Wnt3 based on two patterning systems. Validated using the previous and new experimental data, the models suggest that β-catenin translocation (in interplay with still unknown factors) is involved in the large-scale

formation of the body axis, whereas Wnt3 drives a distinct small-scale pattern formation system responsible for organiser formation, eventually controling small-scale head formation downstream of *β-catenin*. This offers new theoretical insights in pattern formation, which may have important implications for the design and interpretation of future *Hydra* experiments. The results of this study suggest that the control mechanisms may also be more complex in other animals, where canonical Wnt signaling has been assumed to be the main driver of body-axis (including head) formation (65). Given that Wnt/β-catenin-mediated pattern formation is fundamental to animal development, our data might also have implications for higher bilaterians, including humans.

RESULTS AND DISCUSSION

The following results combine data from simulations and analyses of pattern formation models with previous and new experimental data. The first section presents a systematic review of previous experiments, evaluated in the light of our new paradigm of two distinct pattern formation systems for head and body-axis formation and supported by new statistical analyses. Following these observations, the second section introduces a new mathematical model, called ”two-system model”, as an extension of the previous modeling approaches. Using model simulations and analysis, we compare it with a prototype for a single-system model based on the late Meinhardt concept (52; 53), and we present novel model predictions. The third section is devoted to new experimental data that allow closing the conceptual loop by experimentally confirming the model predictions.

Previous experiments and new statistical analyses indicating distinct roles/scales of β-catenin and Wnt3

Extensive experimental data have demonstrated that β-catenin and Wnt3 have distinct roles by acting at different spatial and time scales during *Hydra* patterning. Here we summarize the main experiments and conclusions. For more detail we refer to the Supplemental Information S1.

First, it should be emphasized that the general molecular properties in the context of signaling are different for both molecules: β-catenin is a cell-localized transcription factor in the cytosol and nucleus that can influence the expression of a large number of genes. Wnt3, on the other hand, is a soluble morphogen that can be secreted (albeit possibly with a very short range) into the extracellular matrix (ECM). Taken together, this suggests that β-catenin has a more overarching/general role in pattern formation than Wnt3.

Grafting experiments have shown that grafts from the apical tip (associated with *Wnt3* expression) have qualitatively and quantitatively different properties in terms of induction of new axes/heads in the donor compared with tissue grafts from below

the tip, where *β-catenin*-transcript levels are still high (most likely interacting with other soluble factors to establish a long-range gradient) but *Wnt3* expression is lacking. This suggests the involvement of different signaling factors in both systems (14; 48). The existence of two partially independent but coupled systems is also compelling from a developmental point of view because it guarantees the robust formation and size of the Wnt3-associated organiser. If *Wnt3* expression (and thus organiser formation) depended solely on critical thresholds of β-catenin (as e.g. assumed in (52; 53)), this dependence on absolute values would make the appearance and size of organisers highly non-robust (see details in Supplementary Information S1). Robustness is thus achieved by redundant mechanisms (acting at different scales), which is a well-known principle in various biological contexts (92).

Indeed, temporal and spatial differences between *Wnt3* and *β-catenin* expression have also been demonstrated in several single gene expression studies, showing that *Tcf/β-catenin* expression precedes *Wnt3* expression during several patterning processes in *Hydra*, e.g., (15; 23; 35; 43; 78) – see Supporting Information S1 for further details and references. Transcriptomic and pathway analysis revealed that β-catenin-dependent signaling was involved in diverse molecular, non-molecular, intrinsic and extrinsic processes, indicating a versatile and fundamental role, with Wnt3 being only one of several targets (e.g., Ref. (93)). Indeed, Wnt3 was mainly associated with the formation of the head organiser alone. Taken together, these results suggest that Wnt3 follows β-catenin activity and plays a much less general role during patterning.

Finally, analysis of multi-headed phenotypes resulting from molecular manipulations strongly suggested the existence of two independent patterning systems acting at different spatial scales: A permanent increase in Wnt3 (by knockdown of Wnt3-specific inhibitors such as *Sp5* (90) or *HAS-7* (99)) often resulted in animals with double or multiple heads emanating from the same location – like a split of the original single organiser into two or more organisers/heads in regions (head, budding zone) where β-catenin levels were elevated (90; 99) ('multi-headed phenotype'; Fig. 1 a,e). The same occurred in *Wnt3*-overexpressing animals, although the ectopic head locations were more variable (99) (see discussion below). In contrast, a permanent and global increase in β-catenin resulted in animals with regular branching of new axes (*de novo* axis formation), with a normal distance between the head and the budding zone ('multiple axes phenotype'; Fig. 1 a,d). Thus, in summary, the *Wnt3* overexpression condition can only lead to the formation of new axes/heads from the surroundings of existing organisers, whereas the overexpression of *β-catenin* leads to the formation of new ectopic axes at the maximum distance from the existing organiser.

Statistical analysis of the pairwise distances between the heads in polyps with manipulated β-catenin and Wnt3 levels supported the existence of these two phenotypes: Polyps with increased *β-catenin* expression showed a unimodal histogram similar to a normal distribution (Shapiro-Wilk test: $W = 0.96, p = 0.17$; Fig.1 b), whereas polyps with increased Wnt3 levels (via *Sp5*-knockdown) showed a distinctly bimodal histogram, strongly deviating from a normal distribution (Shapiro-Wilk test:

$W = 0.80$, $p < 0.001$; Fig.1 c). More details of this analysis are given in Supplemental Information S1. A statistical analysis of the number of heads/axes, feet and monotentacles (Fig.1 f) in addition demonstrates that for *Wnt3*-overexpressing animals, the number of heads/axes is significantly higher than the number of feet (confidence intervals do not overlap) whereas in *β-catenin*-overexpressing polyps, confidence intervals strongly overlap. Differences in total numbers of head/axis in both treatments are however related to differences in total polyp length which is not further considered in our study. The phenotypes resulting from overexpression experiments and observations at the tissue level thus indicated that secreted Wnt3 and cytoplasmic/nuclear β-catenin controlled different aspects of *Hydra* patterning.

Notably, a transient increase of β-catenin induced by a high dose of the glycogen synthase kinase-3β inhibitor alsterpaullone (ALP) did not lead to the formation of multiple axes, but resulted in transient expression of multiple *Wnt3* expression spots all over the body, followed by the formation of ectopic tentacles (15; 23) ('tentacle phenotype'; Fig.1 a). ALP prevented β-catenin degradation, resulting in high, body-wide, constant levels of *β-catenin* transcripts (Fig. 1 a). This pattern was not followed by *Wnt3*, which was expressed in a complex arrangement of multiple organiser-sized spots all over the body, demonstrating that the spatial dynamics of Wnt3 were affected by an additional regulatory mechanism. This resulted in qualitatively different expression patterns of *β-catenin* and *Wnt3* acting at distinct spatial scales; however this does not generally exclude an interplay between both components. The combination of ALP treatment with small interfering RNA (siRNA)-mediated knockdown of *Wnt3* led to a reduction in the number of ectopic tentacles, indicating that β-catenin and Wnt3 exerted distinct but partially complementary functions in pattern formation (45). Finally, administration of a lower dose of ALP for a longer time also led to ectopic axes, similar to the *β-catenin*-overexpression phenotype described above (99).

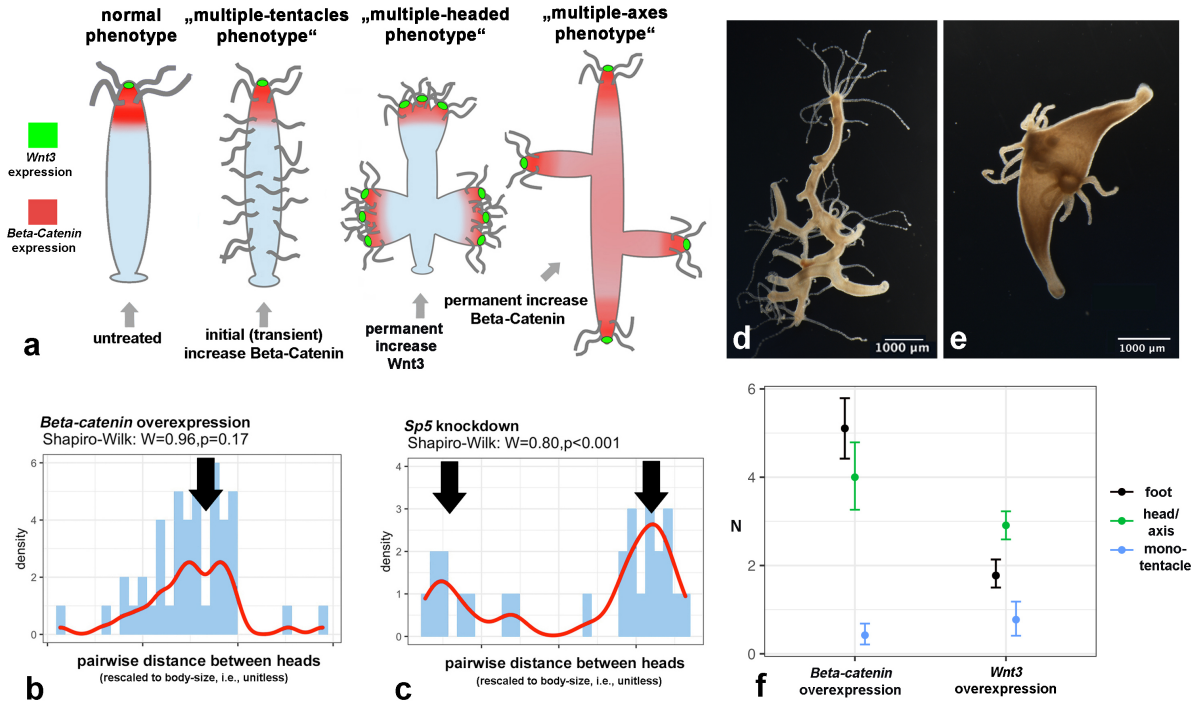

Figure 1. (a) Diagrams of phenotypes for the undisturbed system and following a transient increase in β-catenin, a permanent increase in Wnt3, and a permanent increase in β-catenin, respectively. (b)-(c) Histograms (blue) and density plots (red) of pairwise normalized (i.e., unitless) distances between heads of polyps with increased *β-catenin* (b) and *Wnt3* (c) expression. Black arrows indicate different modes. (d)-(e) Light-sheet images of *β-catenin*- (d) respectively *Wnt3*-overexpressing phenotypes. (f) Statistical analysis of the number of axes/heads, feet and monotentacles, error bars depict 95%-confidence intervals based on bootstrap.

Computational approach to study the respective functions of β-catenin and Wnt3

To investigate the relationship between the body axis and head patterning, we applied two mathematical models: a single-system model based on a single pattern formation loop and the new two-system model coupling two pattern formation loops. Details of the mathematical setup are given in the 'Materials and Methods' section. Here we focus on the introduction of the models, the biological justification of the model structure and the model validation based on experimental data.

A single-system model of body-axis and head patterning

A simple explanation for the spatial-temporal differences between localized expression of *Wnt3* and patterns of *β-catenin* expression at the body column scale could be provided by a mechanism in which β-catenin is part of a signaling loop showing *de novo* pattern formation, with *Wnt3* expression activated above a certain threshold of β-catenin. Such a mechanism has been

proposed in the late model of Meinhardt (52; 53), in which Wnt3 is locally enhanced by an additional loop to explain the difference in size between *Wnt3* and *β-catenin* expression spots. Consequently, axis and head formation were assumed to be driven by a single pattern formation system. However, a systematic simulation of the model shows that it cannot generate stable *Wnt3* expression patterns, and *Wnt3* expression spikes continue to increase over time (see Supplementary Information S3). To further explore the ability of the single-system model to reproduce the experimental data, we reduced the complexity of the model by assuming expression of *Wnt3* arising above a certain critical level of β-catenin and assuming an activator-inhibitor model for β-catenin patterning. In other words, we neglected the additional molecular complexity of Meinhardt's model (52; 53) and formulated a prototype single-system β-catenin/Wnt3 model with a threshold-based mechanism for scale separation (Fig. 1). Simulations showed that this model could not explain the experimentally observed transient *Wnt3* expression spots after ALP treatment (see below and Supplementary Information S3). Furthermore, the single pattern formation structure of the model could not explain the different multi-headed phenotypes (multi-axes vs. multi-headed; see Fig. 1 a) or the independence of *Wnt3* transcript levels following *β-catenin* overexpression (see below).

Two-system model separating body-axis and head patterning

Motivated by the experimental observations described above, which suggest that *Wnt3* expression patterns are regulated by a partially autonomous patterning system rather than being a mere readout of β-catenin activity, we propose a new mathematical model describing the interplay of two distinct but interconnected patterning systems. The aim is to determine if the existence of additional control of Wnt3 pattern formation is sufficient to explain the experimental observations. The proposed model introduces a separate pattern formation control for: (1) the body-axis gradient; (2) the head/organiser pattern. Additionally, these systems are assumed to interact with the long-term storage of the body-axis gradient (head-forming potential / source density (52)). The latter follows the classical motivation by Meinhardt but is also supported by recent experimental observations (87). For additional comparison with experimental data, we extend the model to include tentacle-related patterns. The latter does not contribute to the mechanism of body axis/head formation and is only used to compare the model with the tentacle data.

The novelty of the two-system model is that it zooms out the head/body axis patterning system and explicitly distinguishes between two (interconnected) patterning systems that act differently in the apical region versus the body column. The model assumes that the body-scale patterning system is informed by nuclear β-catenin. This activates, among other things, the production of Wnt3, which in turn is mediated by an additional, independent control loop that provides a head-organising function at the small scale. A scheme of the model is presented in Fig. 2 (b), compared with the scheme of the single-system model (Fig. 2 (a)). Specific interactions between model components, assumptions about model parameters, initial conditions, and information on the simulation code and software are provided in the 'Materials and Methods' section.

The core structure of both, systems of β-catenin and Wnt3 patterning is based on an activator–inhibitor scheme exhibiting Turing instability. The use of the activator-inhibitor schemes within the model does not follow the molecular nature of the patterning process, but substitutes for more complex underlying processes and mechanisms that are not yet well understood at the molecular level. Several chemical (71) and non-chemical (13; 34; 55; 58) alternative pattern formation loops have recently been considered but none of them can be currently verified on the molecular level. For the small-scale (i.e., head-organiser-related) activator–inhibitor pattern formation system, we assume that Wnt3 is part of a signaling loop with a hypothetical inhibitor. The latter can be linked to the recently discovered Sp5 transcription factor, which plays an important role in the transcriptional inhibition of Wnt3 (90). In addition to Sp5, Notum, another Wnt antagonist, is a carboxylesterase that requires glypicans to suppress Wnt signaling by depalmitoleoylation of Wnt proteins (38; 39). Furthermore, this complex network of Wnt antagonists might also include Wnt inhibitors (such as the astacin proteinase HAS-7) that act by cleaving Wnts to inactivate them (98; 99). In the context of the body-axis system, β-catenin is assumed to be part of an activator complex (possibly including additional molecules such as Tcf (35)). Here, one of different possible molecular candidates for the inhibitor complex is Naked cuticle (Nkd) which was shown to be expressed in broad, gradient-like patterns along the body axis resembling *β-catenin/Tcf* expression after ALP-treatment (c.f., below). In addition, Nkd binds to Dishevelled (Dvl) family proteins preventing the translocation of β-catenin into the nucleus (69; 95). However, due to its intracellular nature, the long-range inhibition cannot be explained by this protein alone but requires additional interactions, which can be also of a mechano-chemical, cellular or bio-electrical character (11; 18; 44; 58; 76). Furthermore, interactions between β-catenin and different Dickkopf (Dkk)-molecules may drive self-organization of the *Hydra* body axis (57).

In summary, although there exist several regulators of the Wnt3 and β-catenin dynamics, the related signaling systems are still not sufficiently understood to describe a complete working pattern formation mechanism without hypothetical components. Notably, all these mechanisms fit into the general concept of local activation and long-range inhibition (LALI). In this context, we replace the complex subsystems by simple pattern formation loops, using the inhibitor–activator model as a mathematical description of the LALI scheme. The consideration of patterning systems rather than individual molecules is supported by the fact that we obtained comparable results when replacing entire patterning units in our model by alternative mechanisms, i.e., replacing the activator-inhibitor loop by a mechano-chemical one (see Supplementary Information S4). This is an important observation because we do not view our model as a tool to identify specific interactions at the molecular level, but rather as a tool to investigate the role of β-catenin versus Wnt3 in developmental and regenerative processes in *Hydra*.

Model simulations and comparison to experimental data

Using the proposed two-system model, we simulated a steady-state system and various experimental scenarios induced by ALP treatment, knockdown, or overexpression. The model results were compared to experimental data and to the results of the

single-system model. The results show that both models adequately describe the steady-state scenario and can reproduce the spontaneous head development (Fig. 2 (b) and (d) – undisturbed scenario). The resulting gradient-like patterns of *β-catenin* expression, with a maximum at the head, a small, sharp spot of *Wnt3* expression at the tip of the hypostome, and a ring of tentacles beneath the head, are in agreement with experimental observations. Here, as in all other simulations based on the single-system model, Wnt3 spots appear to be distinctly larger compared to the results of the two-system model. Indeed, smaller spots could be obtained by applying higher β-catenin thresholds for *Wnt3* expression in the one-system model. However, in these cases, Wnt3 appears much later than experimentally observed due to the patterning dynamics of the large scale β-catenin system (which develops gradients relatively quickly compared to a rather slow increase in maximum *β-catenin* levels). This demonstrates the non-robustness of *Wnt3* expression and spot size-dependence on the threshold mechanism.

Simulations with initial conditions corresponding to the ALP treatment reproduced the experimentally observed transient multiple *Wnt3* expression spots (e.g., (15; 23)) in early stages after ALP application in the two-system model, but not in the single-system model (Fig. 1 (b),(d) and Supplemental Information S4). With respect to the ectopic tentacle development (15; 23) and the development of a secondary body axis (e.g., additional file 10; Fig. S 8e in (99)) in later stages after the ALP treatment, the results of both models are similar to experimental observations. The same holds for the simulation of the *β-catenin* overexpression, also leading to the development of a secondary body axis (Fig. 1 (b),(d)).

In addition, we compared the two models with the results of experiments of the *Wnt3* overexpression (99). In the two-system model, the simulated pattern strongly resembles the *β-catenin*-overexpression phenotype in terms of the establishment of a secondary body axis, in accordance with the experimental observations (99). However, the model does not reflect the experimental observation of ectopic tentacles, possibly because it does not consider the interaction of the tentacle system with the other systems in detail. In contrast, the single-system model does not even describe the secondary heads/axes formation, instead showing a much broader *Wnt3* expression spot.

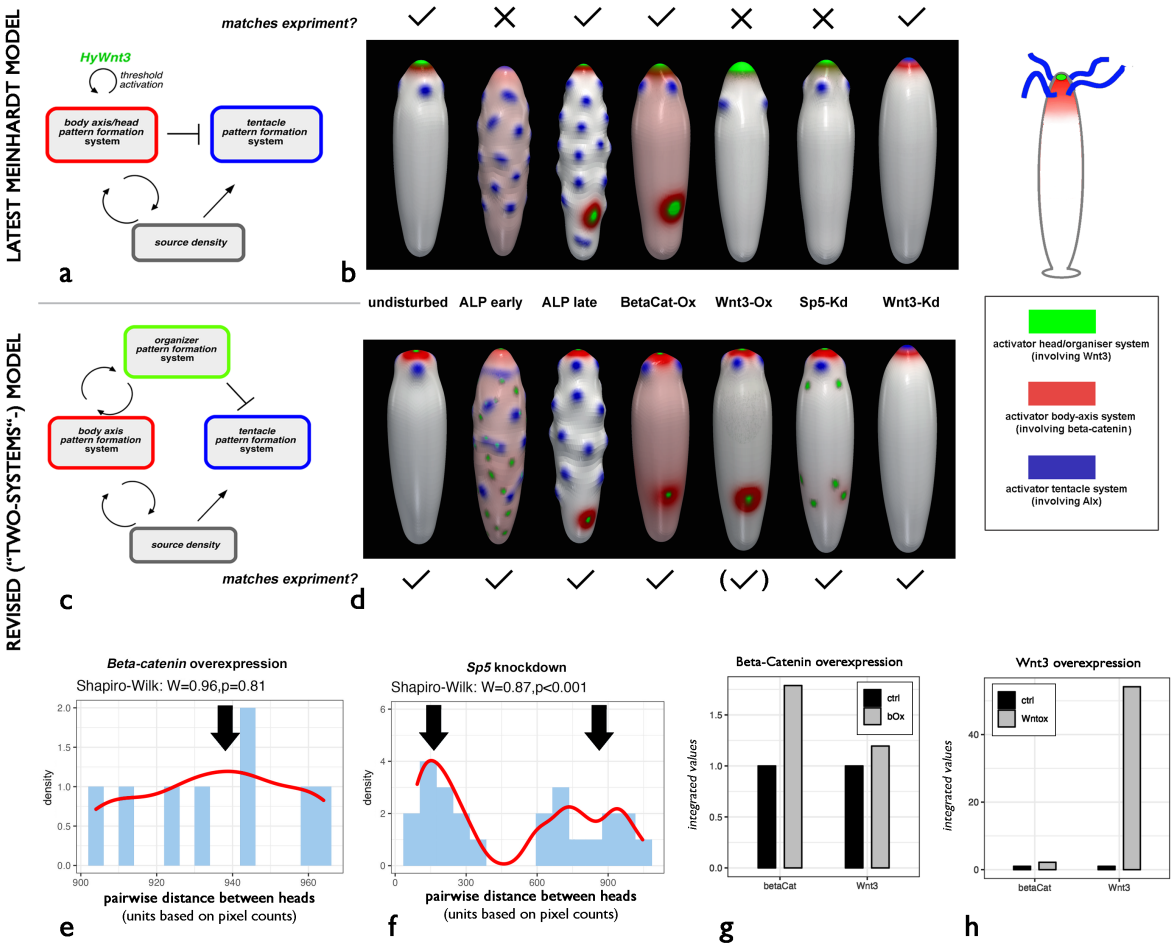

Figure 2. Diagrams of single-system (threshold-based) model (a) and corresponding simulation snapshots of various experimental scenarios (b) and respective diagrams for the proposed two-system model (c, d). Matching patterns between experiments and simulations in (b) and (d) are marked with ticks, otherwise with an X. (e, f) Simulated analogues to Fig. 1 (b,c). Histograms (blue) and density plots (red) of pairwise distances between heads of polyps with increased *β-catenin* (e) and *Wnt3* (f) expression. Black arrows indicate different modes. Integrated total amounts of Wnt3 and *β*-catenin in the simulated *β-catenin*- (g) and *Wnt3*- (h) overexpressing polyps. Values relative to the control (undisturbed) scenarios shown.

Interestingly, in this context, experimental overexpression of potential activators (such as *β-catenin* or *Wnt3* (23; 99)) is usually linked to multi-headed phenotypes. However, a mathematical analysis (Supplemental Information S4) demonstrates that such dynamics cannot be achieved in the context of the classical activator–inhibitor model or even in a wider class of related chemical two-component pattern-formation models. Also, the analysis demonstrates that moderate knockdown of the inhibitor was expected to lead to a multi-headed phenotype, while strong knockdown (i.e., knockout) or strong overexpression of either activator or inhibitor to a complete loss of patterning. In particular, the activator–inhibitor-like models predict that the moderate overexpression of the activator results solely in higher expression levels of the activator molecule, and not in multiple heads (as shown in Fig. 1 (b) for *Wnt3* overexpression). Thus, the experimental observations cannot be explained by models based on a single activator–inhibitor scheme (such as the classical Gierer–Meinhardt model).

Simulated overexpression of *β-catenin* and *Wnt3* in the two-system model led to multiple heads because of the existence of the two distinct patterning systems, mutually connected via the canonical Wnt signaling (and interacting with the source density). In both cases of *β-catenin-* and *Wnt3* overexpression, a positive feedback loop with another supporting component (for Wnt3 the β-catenin system, for the latter the source density) is necessary for the respective system to establish patterns. Thus, our analytical and numerical studies further demonstrate the need to assume two mainly independent patterning systems for axis and head formation, respectively, in order to explain the results of previous experiments - as realized within the two-system model.

The observation that simulated *Wnt3* overexpression does not lead to a ”multiple-headed phenotype” as observed for *Sp5* knockdown, but rather to a ”multiple-axes phenotype” (Fig. 1 (d)), may be initially surprising. However, coupling between the β-catenin-driven large-scale system and the Wnt3-driven small-scale system (due to canonical Wnt signaling) makes the situation more complex and less easy to predict. Notably, *Wnt3* overexpression also activates β-catenin, which together leads to the formation of additional body axes in regions with already relative high β-catenin levels, e.g., the budding zone. In fact, the phenotypes observed experimentally are more variable and may show both ectopic axes and multiple heads. Overall, this suggests that the multiple head and multiple axis phenotypes cannot be used to conclusively assign manipulated molecules to one of the two systems, but rather represent the ends of a scale of possible phenotypes that may be difficult to interpret.

Simulations including knockdown of the Wnt3 inhibitor show multiple Wnt3 spots in both, the head region and the budding zone, when using the two-system model (Fig. 2 (b)), in accordance with observations of the multiple-headed phenotype following *Sp5* knockdown (Ref. (90)). However, the single-system model was not able to reproduce these patterns. Interestingly, in the late stages of simulations based on the two-system model, ectopic Wnt3 spots vanished (not shown), whereas in real experimental systems, they developed into ectopic heads (90). Nevertheless, the ectopic Wnt3 spots persisted significantly longer in the simulated *Sp5* knockdown model compared with simulations including ALP treatment. We concluded that a certain

morphogen-synthesis time is required in the real system, sufficient to initiate a local cell differentiation process. The latter leads to 'fixation' of the organiser and suggests that a transient expression pattern is sufficient to control the process. These effects were not incorporated in our present and previous models, which is why the *Wnt3* expression spots finally vanished following simulated *Sp5* knockdown treatment. For further model validation, we also simulated Wnt3 knockdown using both models (Fig. 2 (b),(d)), which both reproduced the formation of a single tentacle at the outermost tip of the hypostome, in accordance with Ref. (87)).

Finally, we further investigated the interplay between the large- and small-scale systems in the framework of the two-system model by doing predictive modeling, which consisted an important additional validation step closing the loop between theory and experiments. In particular, we simulated (and later experimentally performed – c.f., below) the separate overexpression of each component (β-catenin and Wnt3), and numerically integrated the total amount of each component in the undisturbed vs. overexpression scenarios. The predicted results are given in Fig. 2 (g)-(h). Global levels of the corresponding virtually overexpressed component increased, whereas the respective other component increased only slightly. This observation was most obvious for *Wnt3* overexpression, where a 50-fold global increase led to only a slight increase in β-catenin.

New experiments and experimental model validation

We closed the conceptual loop by experimentally validating the non-trivial predictions of the two-system model. We experimentally analyzed the virtual predictions presented in Fig. 2 (g)-(h) by evaluating the expression levels of *β-catenin* and *Wnt3* in transgenic polyps overexpressing either *β-catenin* or *Wnt3* (3 (d)-(e)). In agreement with our simulations, overexpression of *β-catenin* did not result in a distinct elevation of *Wnt3* and vice versa. Furthermore, this effect was more distinct in the case of Wnt3 compared with β-catenin, in accord with the simulated results. The observation that the other component was at least slightly increased in simulations compared with experiments was probably related to the fact that our model did not incorporate tissue growth related to axis and head formation. Thus, e.g., in *Wnt3* overexpressing animals, additional Wnt3 spots appeared without the "diluting" effect of additional tissue generated from outgrowth (as in the real system). In addition, steady state effects and/or multiple feedback inhibitors may additionally stabilize *β-catenin* and*Wnt3* expression levels in real systems.

Our conclusions regarding the co-existence of two different regulatory mechanisms controling body-column and head formation motivated additional experiments, which showed the co-existence of distinct types of patterns for different genes under the same treatment. Fig. 3 a–c) demonstrates the experimental setting for allocating molecular candidates to either the large-scale body-axis or small-scale organiser system in *Hydra*. One of several potential molecular candidates interacting with β-catenin and being involved in the large-scale system is *HyNkd*, where treatment of polyps with ALP revealed a homogeneous body-wide expression (Fig.3 c) reminiscent of *β-catenin* (15; 23), and thus significantly distinct from the locally restricted,

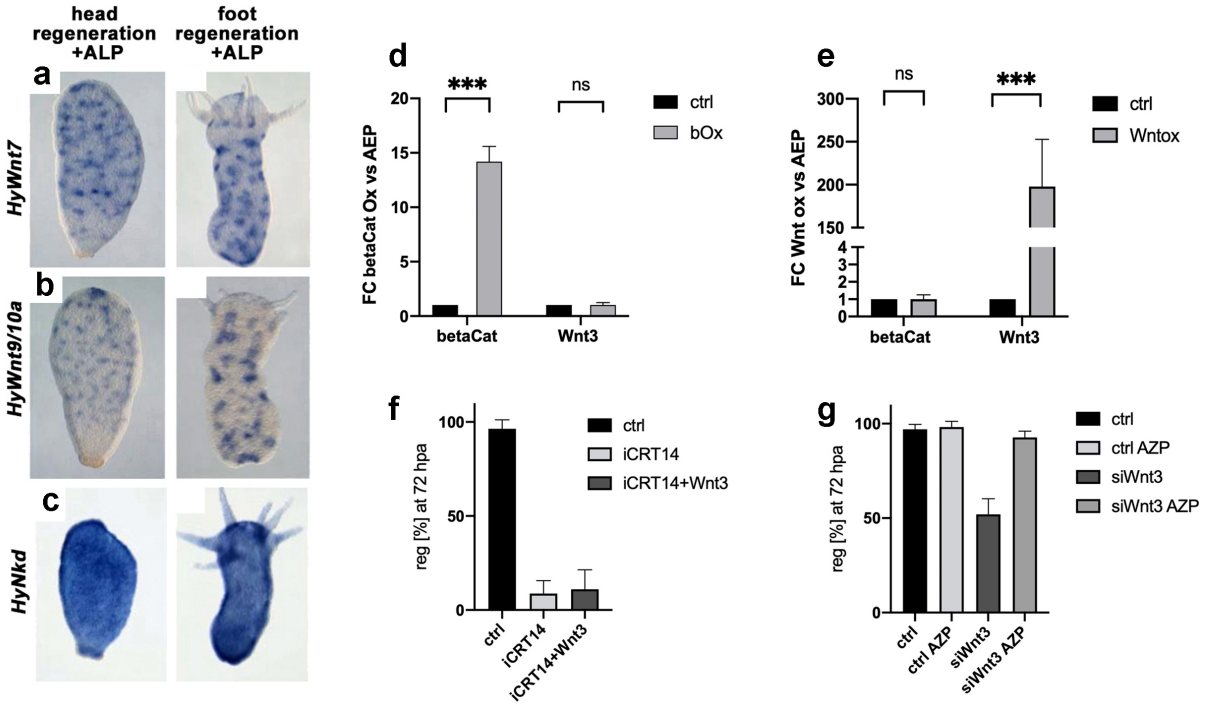

Figure 3. (a–c) Formation of distinct patterns (diffusive vs. spotty) in animals treated with 5 μM ALP, bisected, and evaluated after 72 h, suggesting that expression levels of multiple *Wnts* are regulated differently from other genes such as *HyNkd*. (d) Quantitative reverse transcription-polymerase chain reaction (qRT-PCR) analysis of *β-catenin* overexpressing polyps showed that *Wnt3* transcript levels were not affected and (e) vice versa. (f) Impaired head regeneration following iCRT4 treatment (negatively affecting β-catenin) was not rescued by Wnt3, but (g) regeneration deficiency following *Wnt3* siRNA treatment was rescued by ectopic stabilization of β-catenin using ALP.

small-scale patterns of multiple *Wnts* (Fig.3 a,b). However, due to coupling between β-catenin and canonical Wnts, it might not always be possible to clearly assign molecules to one of the two-system using ALP experiments, analogous to the sometimes difficult interpretation of multi-headed phenotypes (c.f., above). Interestingly, HAS-7 is upregulated globally too by ALP and does not show spot-like distribution (99) which is most probably due to the fact that it is indirectly controlled by β-catenin.

Previous experiments demonstrated the indispensable roles of β-catenin and Wnt3 in head regeneration (31; 87), and we further validated the finding that they had both overlapping and distinct functions by investigating their functional roles in this process. To address this, we determined if the regeneration deficiency following pharmacological (β-catenin) or genetic (Wnt3) reduction could be rescued by reciprocal supplementation by either recombinant Wnt3 protein or ectopic stabilization of β-catenin using ALP (Fig. 3 f–g). When β-catenin-function was blocked by iCRT 14, the regeneration capacity dropped to $<$ 10 %, and this effect was not rescued by parallel incubation with recombinant Wnt3 (Fig. 3 f). This indicates that the role of β-

catenin cannot simply be replaced by Wnt3, in accord with our general conclusion that β-catenin-based body-axis formation is independent of and precedes Wnt3-based head patterning. Conversely, when *Wnt3* function was inhibited by siRNA-mediated knockdown, the regeneration capacity was decreased to 50 % compared with control polyps. Notably, ectopic stabilization of β-catenin by ALP rescued the regeneration-deficient phenotype (Fig. 3 g). However, whether this rescue was directly linked to β-catenin function or indirectly to an increase in other Wnts (43) that might compensate for the loss of Wnt3 remains unclear. Indeed, this rescue might indicate that β-catenin interacts with canonical Wnts other than Wnt3 in order to establish the body axis. Wnt9/10c is a promising potential candidate, given that *Wnt9/10c* knockdown leads to a complete loss of patterns, including tentacles (87).

In summary, these new experiments further support the view that β-catenin and Wnt3 are involved in two separate pattern formation systems, and that the β-catenin-based body-axis system may also involve Nkd, as well as other canonical Wnts (such as Wnt9/10c). Our experimental validation of the proposed two-system model confirmed the non-trivial model predictions.

SUMMARY AND OUTLOOK

In this study, based on a systematic analysis of previous and new experimental data, we proposed a revised two-scale mechanism and a corresponding mathematical model (two-system model) for head and body-axis formation in *Hydra*. Notably, we integrated and re-interpreted the results of previous experiments and datasets, including regeneration and grafting experiments, molecular/chemical manipulations leading to multi-headed phenotypes, analysis of single-gene expression patterns, and transcriptomic data related to β-catenin and Wnt3. We also provided new experimental results targeting the direct interplay and redundancy of nuclear β-catenin and Wnt3, and validated the non-trivial model predictions. In conclusion, β-catenin and Wnt3 appear to act differently in various aspects during *Hydra* patterning, with distinct spatial, temporal, and experimental contexts, suggesting the existence of an independent control mechanism beyond the simple β-catenin-threshold-dependent activation of Wnt3.

We therefore proposed a mechanism involving a core system controling the formation of the body-axis gradient based on β-catenin (in interaction with other possible factors such as Nkd, Wnt9/10c, or further Wnts except Wnt3), with Wnt3 involved in an extra pattern formation system, acting at a smaller spatial scale, which locates and defines the head organiser. Both systems are probably coupled via canonical Wnt signaling, although our quantitative analyses only revealed a weak direct link, with overexpression of each component not influencing the transcript levels of the other component. Simulations of the new two-system model demonstrated its ability to explain a range of experimental observations that could not be described by a classical single activator–inhibitor loop, such as the development of two different multi-headed phenotypes (”multiple-axes” and ”multiple-headed” phenotypes, based on *β-catenin*-overexpression and *Sp5*-knockdown, respectively), *Wnt3* overexpress-

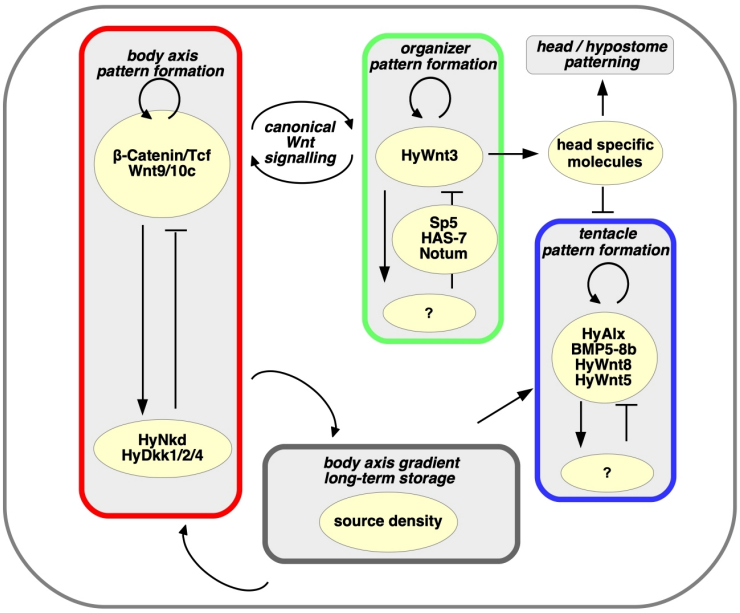

Figure 4. Possible molecular candidates for the two-system model.

ing phenotypes, as well as transient patterns during ALP treatment. Indeed, our analysis of a broad class of pattern formation models confirmed that a single two-component pattern formation system (such as the activator–inhibitor model) cannot explain the experimentally observed multi-headed phenotypes resulting from overexpression of an activator molecule.

We therefore concluded that there are two separate (but coupled) patterning systems for head and body-axis formation, respectively. This paradigm shift has potentially important implications for the design and interpretation of previous and future experimental studies. This represents the first report of this novel concept, reflected by the fact that several recent papers investigating the molecular basis of *Hydra* patterning fail to distinguish between axis and head formation.

One of the main experimental implications of the proposed paradigm shift relates to the search for mechanisms leading to self-organized head/axis formation (such as molecules fitting the activator–inhibitor model): the search for a single pattern-forming mechanism is doomed to failure if there are actually two separate mechanisms, whose players have previously been mixed or equated, making interpretation of the experimental results difficult or impossible. The design and interpretation of future experiments should thus distinguish between the body-axis β-catenin and the small-scale Wnt3 systems. Indeed, candidate inhibitor molecules have recently been identified for the Wnt3 patterning system (such as Sp5 (90) or HAS-7 (99)), although the long-range mechanisms required for the activator–inhibitor principle remain elusive. In contrast, details of the inhibitor molecules for the large-scale, β-catenin-driven body-axis system are still missing, although this patterning step is probably

more fundamental and occurs before the formation of the head. Further studies are needed to investigate the roles of Nkd, the Dkk1/2/4 molecules (2; 30; 57), and Wnt9/10c (43; 87) in this respect. An overview of possible molecules involved in the scheme suggested by the two-system model is given in Fig. 4.

Future experiments involving systematic knockdown or knockout of different genes could also be used to investigate the molecular candidates that interact with β-catenin and the molecules that are dispensable for self-organization of the body axis. Notably, recent experiments indicated that, in addition to diffusing chemicals, physical cues such as discrete cellular nearest neighbor interactions (10; 22; 40; 61; 75), tissue mechanics (11; 18; 44; 58; 76), the extracellular matrix (88; 89), and bio-electrical processes (12) all actively contributed to pattern formation in *Hydra*. The integration of non-diffusive and diffusive signals thus offers a viable alternative to the classical Turing theory of *de novo* pattern formation and may have important consequences for experimental studies.

In summary, the molecular basis of canonical Wnt signaling established in previous decades (3; 36) clearly indicated a crucial role for Wnt in head and body-axis development, in both *Hydra* (35) and higher organisms (65). However, previous models failed to distinguish between body-axis and head formation in the context of canonical Wnt signaling. In contrast, employing a combination of mathematical modeling and simulations using previous and new experimental data, the current study provides the first evidence indicating that these two systems are controlled by two distinct self-organising processes. These two systems are coupled via the canonical Wnt signaling pathway, which ensures continuous alignment of the head with the body axis.

In 2012, based on over 40 years of research into *Hydra* pattern formation, Alfred Gierer noted that even a detailed knowledge of the molecules involved in *Hydra* pattern formation was not sufficient to explain the resulting spatial structures (25). We posit that the patterns that arise can be understood from an interdisciplinary perspective, integrating different chemical and physical processes and principles at the molecular, cellular, and tissue scales (11; 25). Further refinement of our models by integrating the results of different biological, biophysical, and biochemical disciplines will help to clarify the mechanisms driving self-organized pattern formation during development, as one of the key mysteries of biology.

AUTHOR CONTRIBUTIONS

MM designed the conceptual models and integrated them into the computational 3D framework, performed all 3D simulations, carried out the systematic experimental review, and developed the main research questions. AM-C and MM designed, guided and integrated the supporting experimental, numerical and analytical work. MM, AM-C, FV, and AK wrote the manuscript with input from all authors. FV performed the analytical studies and AK performed the numerical 1D analyses. TWH and SÖ conceptually accompanied the experimental work and interpretation. AT carried out the main experimental work, supported by

SH and TL. AM-C, TWH, and SÖ conceived the experimental-theoretical interplay and were in charge of overall direction and planning.

ACKNOWLEDGEMENTS

This work was supported by Deutsche Forschungsgemeinschaft (DFG) under Germany's Excellence Strategy EXC-2181/1 - 390900948 (the Heidelberg STRUCTURES Excellence Cluster) and SFB1324 (B05 to A.M-C and M.M., B07 to SÖ, and A05 to T.W.H). We thank Yukio Nakamura for preparation of the actin::Wnt3 pBSSA-AR vector and initial transgenic *Hydra vulgaris* AEP strains (DFG-FOR 942; T.W.H).

MATERIAL AND METHODS

RESOURCE AVAILABILITY

Lead contact

Further information and requests for resources and reagents should be directed to and will be fulfilled by the lead contact, Moritz Mercker (mmercker_bioscience@gmx.de).

Materials availability

- Does not apply.

Data and code availability

- Datasets composed of Cell Press standardized data types do not apply in the current study.
- All original code for simulations will be deposited online and will be publicly available as of the date of publication. DOIs will be listed in the key resources table.
- Any additional information required to reanalyze the data reported in this paper is available from the lead contact upon request.

EXPERIMENTAL MODEL DETAILS

Hydra culture

Polyps were kept at 18° C in *Hydra* medium (1 mM $NaHCO_3$, 1 mM $CaCl_2$, 0.1 mM KCl, 0.1 mM $MgCl_2$, 1 mM Tris; pH 6.9) and were fed regularly three times a week with freshly hatched *Artemia salina nauplii*. The medium was changed daily. Animals were starved for 24 h prior to experiments. *Hydra vulgaris* AEP was used for all experiments, unless otherwise indicated. *Wnt3*-overexpressing polyps carried a *Hydra actin* promoter driving the expression of *Wnt3*. Transgenic *β-catenin* animals possessed additional copies of a *β-catenin* promoter-driven *β-catenin green fluorescent protein* fusion construct. Generation of both transgenic lines has been reported elsewhere (62). Phenotypical analysis and imaging was performed with bCat-Tg animals that carry an actin-driven bcatenin expression construct. The animals were a kind gift of Bert Hobmayer and have been initially described in Gee et al. (https://doi.org/10.1016/j.ydbio.2009.12.036)

RNA isolation and cDNA synthesis

Polyps were dissolved in 1 mL Trizol (Thermo Fisher) and 0.2 mL chloroform (Sigma-Aldrich). After centrifugation at 12,000 x g at 4 °C, the upper phase was transferred into a fresh tube and mixed with chloroform:isoamylalcohol at a ratio of 24:1. Samples were spun again as above and the upper phase was transferred into a fresh tube. RNA was precipitated with 0.8 volumes of pure isopropanol. After centrifugation, the pellet was washed again in 75 % v/v ethanol, dried in air, and taken up in nuclease-free water. RNA was digested with 1.5 U DNase I (Roche/Sigma-Aldrich) and subsequently inactivated according to the manufacturer's instructions. The quality and concentration of the RNA were examined by 1 % w/v agarose (Invitrogen) gel electrophoresis in 1x TAE using a NanoDrop photometer. cDNA was transcribed using 1 μg RNA and a sensiFAST cDNA Synthesis Kit (Bioline/Meridian) following the manufacturer's instructions.

Quantitative RT-PCR

cDNA was diluted 1:10 in nuclease-free water and used for qRT-PCR using a SensiFast^{TM}SYBR HiROX Kit (Bioline/Meridian) according to the manufacturerÂ´s instructions. Data were normalized to the housekeeping gene glyceraldehyde 3-phosphate dehydrogenase (GAPDH) and evaluated using the ΔΔCt method. All experiments were run in biological and technical triplicate. Results were visualized using GraphPad Prism 8 and tested for significance using t-tests. Wnt3 forward: 5'- ATTACAACAGC-CAGCAGAGAAAG -3'; Wnt3 reverse: 5'- TTATCGCAACGACAGTGGAC -3'; β-cat forward: 5'- AAGTCAGCGTGCTA-GAACAG -3' β-cat reverse: 5'- TGGTTCAGCAAGACGTTGAG -3'; GAPDH forward: 5'- GAGCATCCTGATATTGAAAT-TGTTC -3', GAPDH reverse: 5'- CATGGTATTTCTTTTGGGTTTCTAA -3'

siRNA-mediated knockdown

Hydra vulgaris AEP were collected in petri dishes and rinsed in ddH2O. Twenty animals were placed in a 0.4 cm gapped cuvette (Bio-Rad) and 3 μM siRNA diluted in ddH2O in a total volume of 200 μL was added to the polyps. To increase knockdown efficiency, a combination of two siRNAs for *Wnt3* was used. Electroporation (Bio–Rad Gene Pulser Xcell) was performed with a square wave pulse at 250 V for 30 ms. Restoration buffer (80 *Hydra* medium, 20 dissociation medium) was applied directly after the pulse, and the polyps were subsequently transferred into petri dishes containing chilled restoration buffer. The restoration buffer was partially replaced by HM on the following day, and completely replaced at 2 days post-electroporation. Polyps were allowed to recover from electroporation for 6–7 days and were fed daily during that time. After recovery, the polyps were bisected at 75 % body length and regeneration was evaluated at 72 hpa. For rescue experiments, decapitated polyps were incubated with 2 nM azakenpaullone (Sigma Aldrich) in *Hydra* medium for 24 h immediately after bisection. Green fluorescent protein siRNA (control): 5'–GGUGAUGCAACAUACGGAA_UU–3', siWnt3_A: 5'GGUGAUGCAACAUACGGAA_UU–3', siWnt3_B: 5'–AGAGGCUAUAACGUUAAUA_UU–3'.

Regeneration following iCRT14 treatment

Polyps were pre-incubated with 1μM iCRT 14 in *Hydra* medium for 30 min prior to decapitation at 75 % body length. After bisection, regenerates were transferred into modified *Hydra* medium containing 5 % v/v D-MEM (Gibco; Thermo Scientific; stock solution supplemented with 10 % v/v foetal bovine serum,; Gibco) and 20 μg/mL recombinant Wnt3 protein (Peprotech) or bovine serum albumin (Roth) supplemented with 1 μM iCRT 14. Positive controls were kept in the same medium without iCRT 14. Regeneration was evaluated at 72 hpa and documented with a Nikon SMZ-25 stereomicroscope.

Whole-mount in situ hybridisatin

ALP-treated animals were exposed to 5 μM ALP in *Hydra* medium in the dark for 24 h. ALP was then removed by three washes in *Hydra* medium and the polyps were subsequently bisected at 50 % body length and allowed to regenerate for 72 h prior to fixation. Polyps for whole-mount in situ hybridisatin were relaxed in 2 % w/v urethane in *Hydra* medium for 2 min at room temperature and subsequently fixed in 4 % w/v paraformaldehyde/ PBT at 4°C overnight. WISH was executed using DIG-labelled RNA probes (Roche), as described previously (7; 43).

MATHEMATICAL MODEL AND SIMULATION DETAILS

Definition of the model domain

The cell bilayer is at any time t approximated by a closed 2D surface ellipsoid $\Gamma(t)$, embedded in 3D space. The evolution of $\Gamma(t)$ is given by a diffeomorphic time-dependent representation $\vec{X}$, parameterized over the unit sphere $S^2 \subset \mathbb{R}^3$. Thus, $\Gamma(t)$ is the

image of $\vec{X}(\cdot, t)$ with $\vec{X}(\vec{s}, t) : S^2 \times [0, T] \to \mathbb{R}^3$ for a $T \in \mathbb{R}_{>0}$. Local concentrations of different gene products at time t are given by a set of continuous functions Φ_i, $i = 1, ..., n$, on the deforming tissue surface $\Gamma(t)$, defined as gene product concentrations per cell volume, $\Phi_i(t) : \Gamma(t) \to \mathbb{R}_{\geq 0}$. In order to achieve a consistent formulation with chemical processes being defined on S^2 rather than on Γ, Φ_i are redefined accordingly. This can be achieved because we can identify material points $\vec{X}(\vec{s}, t)$ on $\Gamma(t)$ with $\vec{s} \in S^2$, because $\vec{X}$ is smooth and bijective. Thus for each $\vec{s} \in S^2$, $t \in [0, T]$, we define functions $\Phi_i : S^2 \times [0, T] \to \mathbb{R}_{\geq 0}$ by $\Phi_i(\vec{s}, t) = \Phi_i(\vec{X}(\vec{s}, t))$.

Mathematical setting

The model is given in terms of partial differential equations (PDEs) accounting for spatio-temporal interactions among the signaling factors defined on an evolving domain representing the tissue. Application of a continuous modeling approach is justified by the large number of cells ($\geq 5 \times 10^4$) in the system (81). The choice of model geometry is motivated by a realistic description of the tissue as a radially symmetrical ellipsoid undergoing small deformations due to changes in gene expression patterns. To describe its dynamics, we adopt a mechano-chemical modeling approach as proposed in Ref. (56; 58; 59). The signaling systems are described by reaction–diffusion equations describing defined on a curved 2D surface embedded in a 3D space. The geometry of the curved surface is assumed to evolve according to a gradient-flow of Helfrich-type energy, reflecting the fact that bending of the tissue away from a preferred local curvature is energetically unfavourable. Small tissue deformations are assumed, e.g., follow patterns of gene expression in the initial phase of tentacle development. In contrast to the fully coupled mechano-chemical model of (58), the main version of our presented model (for a mechano-chemical alternative, c.f., below) does not consider any feedback between the mechanical properties of the tissue and the gene expression. In Ref. (58), we considered axis formation in mechanically oscillating *Hydra* re-aggregates of dissociated cells, which were described to require mechanics for patterning. In contrast, the current study focuses on axis vs. head formation in *Hydra*, which also comprises processes such as head regeneration, homeostasis, and budding. However, it remains unclear whether the mechanical stretching in aggregates is an artefact of the sphere-like reaggregates lacking a preformed mouth opening characteristic of intact animals, so the mechanical stress may not be essential for *Hydra* axis formation in general. Thus, for the sake of simplicity, we neglect the role of tissue stretching and consider a pattern formation process based solely on molecular interactions.

To demonstrate the robustness of the model results with respect to the choice of the pattern formation mechanism underlying each sub-system, we developed a second version of the model, relying on similar qualitative interactions between the different pattern formation systems but using different mechanisms for β-catenin and Wnt3 *de novo* pattern formation itself (c.f., Supplemental Information S3). Motivated by the increasing experimental evidence that tissue mechanics may actively influence axis formation (11; 44; 58), particularly *Wnt3* expression (18) in *Hydra*, we replaced the activator–inhibitor scheme by a a mechano-chemical model where *Wnt3* expression and tissue curvature are coupled in a positive feedback loop (56).

Variable name	Explanation
β_cat	Nuclear β-catenin, possibly linked to other factors such as Tcf and/or Wnt9/10c (43; 87)
β_cat_{ant}	β_cat antagonist (presumably linked to Dickkopf1/2/4-C (2; 52; 57) and/or HyNkd)
$Wnt3$	Wnt3
$Wnt3_{ant}$	Wnt3 antagonist (related to Sp5 (90), HmTSP (45), or Notum signaling)
$Head$	Head-related factors downstream of Wnt3 (e.g., multiple Wnts (43))
SD	Source density (long-term storage of head-forming potential (87))
$Tent$	Tentacle activator (may involve HyAlx (74), Wnt8, and Wnt5 (66) or BMB5-8b (68))
$Tent_{ant}$	Tentacle activator antagonist (unknown)

Table 1. Model variables and possible molecular representatives.

Furthermore, for the *de novo* formation of the body axis, we replaced the Turing mechanism by the mutual inhibition model recently presented by (57) (further details are given in Supplemental Information S3).

Interactions between molecule groups

In the two-system model, we considered eight different groups of molecules Φ_i (denoted in the following, if known, by its most prominent representatives), where five groups build the core pattern formation system explaining axis vs. organiser formation (namely β_cat, β_cat_{ant}, $Wnt3$, $Wnt3_{ant}$, and SD) and three components are augmented to include further head and tentacle development (namely $Head$, SD, $Tent$, and $Tent_{ant}$). However, the latter were not required for all the main statements of this work, given that the interplay with the tentacle system was not the main focus of the study. An overview of possible molecular candidates is given in Table 1. Here, β_cat and β_cat_{ant} represent the activator and inhibitor associated with the body-axis patterning system involving nuclear β-catenin. $Wnt3$ and $Wnt3_{ant}$ are the activator and inhibitor of the Wnt3 organiser pattern formation system, respectively. $Head$ is one of several head-specific gene products downstream of the organiser (such as one of the multiple head-specific Wnts (66)), SD denotes the source density, and $Tent$ and $Tent_{ant}$ describe the activator and inhibitor of the tentacle system, respectively. The PDE system describing interactions among these components is given in Eqs. (0.0.1)-(0.0.5) (core system) as well as Eqs. (0.0.6)-(0.0.8) (head and tentacle system), where $\Delta^{\Gamma}(.)$ denotes the surface Laplace (Laplace–Beltrami) operator, and d_t stands for time-derivative. Specifically, Eqs. (1)–(2) describe the body-axis pattern formation system, Eqs. (3)–(4) describe the organiser pattern formation system, Eq. (5) is for the source density, Eq. (6) describes the equation for $Head$, and the tentacle system is given by Eqs. (7)–(8).

Although β-catenin is a non-diffusive molecule, we modelled the pattern formation system of β-catenin using a system of reaction–diffusion equations, because it might interact with other (possibly diffusing) ligands, such as Wnt9/10c. The diffusion-based model can also be seen as an abstract representation of a more complex pattern formation model in which effective short-range cell-to-cell communication may be realized through interactions with Wnt signaling (3). A mechanism of pattern

formation exhibited by components of intracellular signaling coupled to a single diffusive component has been demonstrated in a series of mathematical works (32; 49). The desired pattern formation mechanism can be also realized by the interplay between β-catenin and mechanical cues. The formation of morphogen patterns in the absence of lateral chemical diffusion has recently been demonstrated in simulation studies based on a mechano-chemical model (13). Considering several possible molecular mechanisms that could explain the formation of the β-catenin patterns, we formulated the current model in terms of a reduced mathematical metaphor for such mechanisms. A similar modeling strategy was applied in the seminal works of Meinhardt (51; 52). In particular, we assumed that *β-catenin* expression requires the source density (52; 87) and, due to canonical Wnt signaling, is additionally supported by Wnt3.

The extension of the current model compared with previous models includes a separate activator–inhibitor system for the Wnt3 organiser system and the additional variable $Head$, which represents the head-specific molecules expressed downstream of the organiser, in order to fine-scale the pattern of the *Hydra* head region (e.g., multiple Wnts (43)). The activator–inhibitor system for Wnt3 is modelled as a small-scale pattern formation system with saturation of its own expression, motivated by the sizes and spacing of the (transient) Wnt3 spots after ALP treatment. The production of Wnt3 is assumed to require β-catenin. Wnt3 again activates head-specific molecules ($Head$), but only above a certain threshold, $thresh = 5.0$. We introduced this threshold to account for the assumption that head construction only starts if the organiser is well established. $Head$ is again assumed to negatively influence the tentacle system. This negative influence of the *Hydra* hypostomal region on the tentacle system has been demonstrated in different experiments (68; 74; 80).

The large total number of variables/fields in the presented model may lead to the criticism that the model includes "...so many parameters that they can made to fit anything..." (46). Notably however, only equations (1)–(5) are required to reproduce the main results of this study. In addition, most parameters in Eqs. (1)–(8) are not critical for the qualitative simulation results presented in this study; most of them control specific properties of one of the three considered *de novo* pattern formation systems, such as spatial scaling in general, spacing between appearing maxima, or the condition required to start the *de novo* patterning process. Most of these parameter have been adopted from Ref. (51; 52). They are not within the focus of the current study and do not critically influence our main results, given that general interactions between the different pattern formation systems in *Hydra* are considered, rather than the details or the *de novo* pattern formation systems themselves (c.f., Supplemental Information S4).

The detailed molecular mechanisms responsible for the latter are still elusive and need further research, but are beyond the scope of the current study. The activator–inhibitor model has thus been used just as an appropriate "toy-model". The main focus of this study was therefore the aspects of *Hydra* patterning that do not depend on the specific choice of *de novo* patterning mechanisms, including the existence and interplay of the different patterning systems, rather than the identification of specific

molecular interactions that could fit to a specific pattern formation mechanism.

We therefore believe that our main conclusions were largely unaffected by most of the model parameters. Because the simulation times required for a systematically numerical robustness analysis for our models are not feasible, we demonstrated this robustness by developing and simulating an alternative model relying on similar proposed scales and interactions between the distinct pattern formation systems, but realizing *de novo* patterning for each single system in completely different ways. More details are given in the Results and Discussion and in Supplemental Information S4.

Core pattern formation system:

$$d_t\beta_cat = a_1\Delta^{\Gamma}\beta_cat + b_1 \cdot (c_1 Wnt3 + SD \cdot \frac{0.05 + \beta_{cat}^2}{\beta_cat_{ant}}) - d_1 \cdot \beta_cat \tag{0.0.1}$$

$$d_t\beta_cat_{ant} = a_2\Delta^{\Gamma}\beta_cat_{ant} + b_2 \cdot SD \cdot \beta_{cat}^2 - d_2 \cdot \beta_cat_{ant} \tag{0.0.2}$$

$$d_t Wnt3 = a_3\Delta^{\Gamma} Wnt3 + b_3 \cdot \beta_cat \cdot \frac{0.005 + Wnt3^2}{Wnt3_{ant} \cdot (1.0 + c_3 \cdot Wnt3^2)} - d_3 \cdot Wnt3 \tag{0.0.3}$$

$$d_t Wnt3_{ant} = a_4\Delta^{\Gamma} Wnt3_{ant} + b_4 \cdot \beta_cat \cdot \frac{0.005 + Wnt3^2}{1.0 + c_4 \cdot Wnt3^2} + 0.06 - d_4 \cdot Wnt3_{ant} \tag{0.0.4}$$

$$d_t SD = a_8\Delta^{\Gamma} SD + b_8 \cdot \beta_cat + 10^{-4} - d_8 SD. \tag{0.0.5}$$

Additional equations for further head and tentacle formation:

$$d_t Head = a_5\Delta^{\Gamma} Head - d_5 Head + \left(b_5 Wnt3\right)\Big|_{Wnt3>thresh} \tag{0.0.6}$$

$$d_t Tent = a_6\Delta^{\Gamma} Tent + \frac{b_6 \cdot SD \cdot (0.005 + Tent^2)}{Tent_{ant} \cdot (1 + c_6 \cdot Tent^2) \cdot (1 + e_6 \cdot Head)} - d_6 \cdot Tent \tag{0.0.7}$$

$$d_t Tent_{ant} = a_7\Delta^{\Gamma} Tent_{ant} + \frac{b_7 \cdot SD \cdot (0.005 + Tent^2)}{(1 + c_7 \cdot Tent^2) \cdot (1 + e_7 \cdot Head)} + 0.014 - d_7 \cdot Tent_{ant} \tag{0.0.8}$$

Single-system model

The considered single-system model is based on the late Meinhardt model (52; 53), which however does not lead to stable patterns (Supplemental Information S3) and moreover consists of too many equations that are not needed to describe the core dynamics. Based on the proposed Mainhard's idea, we extract a basic single-system model by reducing its complexity using Eqs. (1)–(8), but replacing Eqs (2)–(3) by one equation for Wnt3 assuming *Wnt3* expression above a certain critical threshold of β_cat.

Tissue curvature

The chemical/molecular equations Eqs. (1)–(8) are augmented by a set of equations representing the deforming tissue surface. Notably, we treat the tissue as purely elastic, and elastic tissue deformations were based on minimization of the Helfrich free energy (33), given by

$$\mathcal{F}_{bend} = \int_{\Gamma} \kappa (H - H_0(\beta_cat, Tent))^2 \, d\vec{S}.$$

Here, H is the mean curvature, κ the bending rigidity, and H_0 the spontaneous curvature (56; 59). H_0 represents the locally preferred tissue curvature, which again may depend on local morphogen concentrations. Here, we assume $H_0(\beta_cat_{ant}, Tent) = 0.5 \cdot \beta_cat_{ant} + 15. \cdot Tent$, based on the observation that local tissue evaginations can be observed during both budding and tentacle formation (1; 66). Local area-conserving evolution of the deforming *Hydra* tissue is finally given by the L^2-gradient flow of the total energy. Further details are given in Ref. (59).

The model proposed in this study focuses on the interplay of pattern formation feedback loops in the biochemical signaling system, and simulated changes in tissue curvature are thus only a read-out of biochemical morphogen concentrations. We include the resulting evolution of the tissue geometry in our model (through a respective PDE describing tissue mechanics), because even the dynamics of a purely biochemical model depend on the domain size and geometry that may influence the appearance and spacing of the organising centres. Various theoretical studies have demonstrated that Turing-type patterns depend directly on the underlying geometry leading, e.g., to spots on the body and stripes on the tail during animal coat patterning. We therefore consider that the interaction of biochemical patterning and tissue geometry, which approximates the real geometry, is important for obtaining realistic patterns. This allows for a more realistic description of tentacle formation in our model, which can again be used for further model validation (e.g., simulating ALP treatment). However, exemplary simulations without tissue deformations reveal only minor differences, suggesting that tissue geometry plays only a subordinate role (Supplemental Information S3).

We previously demonstrated (43; 66) that Wnt5 and Wnt8 acted downstream of canonical Wnt 3 and Wnt9/10 signaling. Wnt5 acts as a non-canonical Wnt signal during tentacle formation, and non-canonical Wnts are known to be involved in planar cell polarity, which is in turn closely linked to changes in cell geometry. Downstream of non-canonical Wnt signaling during tentacle outgrowth, *Hydra* Alx-spots change from spots to rings (74), probably caused by the interplay between chemistry and geometry. Nevertheless, although there is likely to be an interplay between chemical signaling and the underlying evolving tissue geometry, strong geometric changes were not considered in the present study because they seemed to be irrelevant to the mechanism of axis formation per se.

Simulation method

For simulations of the model, we use the finite element library Gascoigne (5), approximating the fourth order PDEs in a mixed formulation. For spatial discretization, we use linear finite elements (including local mesh refinement in areas with strong local curvatures), and for time discretization, we use a semi-implicit Euler scheme (including an adaptive time-step scheme). Further details of the computation scheme are provided in (56; 59).

Parameters and initial conditions

For simulations of the undisturbed system, most of the parameters are adapted from Ref. (51; 52). For the unperturbed system, we use: $a_1 = 9 \times 10^{-5}, b_1 = d_1 = 3 \times 10^{-3}, a_2 = 1.1 \times 10^{-2}, b_2 = 3 \times 10^{-3}, d_2 = 4 \times 10^{-3}, a_3 = 2.25 \times 10^{-5}, b_3 = 4.8 \times 10^{-2}, c_3 = 1.8 \times 10^{-3}, d_3 = 1.2 \times 10^{-2}, a_4 = 0.9 \times 10^{-3}, b_4 = 0.72 \times 10^{-1}, c_4 = 1.8 \times 10^{-3}, d_4 = 1.8 \times 10^{-2}, a_5 = 5 \times 10^{-4}, d_5 = 1 \times 10^{-2}, b_5 = 1, a_6 = 7.5 \times 10^{-5}, b_6 = 2 \times 10^{-2}, c_6 = e_6 = 1 \times 10^{-1}, d_6 = 2 \times 10^{-2}, a_7 = 3 \times 10^{-3}, b_7 = 3 \times 10^{-2}, c_7 = e_7 = 1 \times 10^{-1}, d_7 = 3 \times 10^{-2}, a_8 = 1.1 \times 10^{-4}, b_8 = d_8 = 1 \times 10^{-4}$. To approximate the *Hydra* shape, initial conditions for X_1, X_2, and X_3 are parameterized over the closed 2D unit-sphere S^2 embedded in 3D space with $X_1(t = 0) \equiv X_2(t = 0) \equiv 0$ and $X_3(t = 0) = 4 \cdot s_3$, thus leading to stretch in the direction of s_3 (given that s_1, s_2, s_3 are Eulerian coordinates of the S^2 surface). For chemicals, we use a stochastic initial distribution based on the standard random generator provided by C++. The only exception is the source density, which is provided with an initial gradient, namely via $SD(t = 0) = 4.0 \cdot (exp(s_3)/exp(1))$. Thus, in all simulations, chemical patterns follow stochastic initial conditions, with only the geometric and chemical body-axis gradient initially provided. For simulations including ALP treatment, the initial conditions for the source density are changed by adding an offset by $SD(t = 0) = 2.0 + 4.0 \cdot (exp(s_3)/exp(1))$. *Sp5* knockdown is simulated by increasing degradation of *Wnt3_ant* by multiplying d_4 by the factor 1.7, and overexpression of *β-catenin* and *Wnt3* are realized by adding the constant $c = 0.003$ to the right-hand side of the corresponding equation.

SUPPLEMENTAL MATERIALS

- Pdf-document with text and figures (”SI.pdf”)

References

1. R. Aufschnaiter, R. Wedlich-Söldner, X. Zhang, and B. Hobmayer. Apical and basal epitheliomuscular F-actin dynamics during bud evagination. *Biol. Open*, 6:1137–48, Aug. 2017.

2. R. Augustin, A. Franke, K. Khalturin, R. Kiko, S. Siebert, G. Hemmrich, and T. C. G. Bosch. Dickkopf related genes are components of the positional value gradient in Hydra. *Dev. Biol.*, 296:62–70, Aug. 2006.

3. N. Barker. The canonical Wnt/beta-catenin signalling pathway. *Mol. Biol.*, 468:5–15, 2008.

4. L. Beccari, N. Moris, M. Girgin, D. A. Turner, P. Baillie-Johnson, A.-C. Cossy, M. P. Lutolf, D. Duboule, and A. M. Arias. Multi-axial self-organization properties of mouse embryonic stem cells into gastruloids. *Nature*, 562:272–276, Oct. 2018.

5. R. Becker, M. Braack, T. Dunne, D. Meidner, T. Richter, and B. Vexler. Gascoigne 3D- a finite element toolbox (http://www.gascoigne.uni-hd.de). 2005.

6. H. R. Bode. Head regeneration in Hydra. *Dev. Dyn.*, 226:225–36, 2003.

7. H. R. Bode. Axial patterning in Hydra. *CSH Perspect. Biol.*, 1(1):a000463, Jul 2009.

8. H. R. Bode. Axis formation in Hydra. *Annu Rev Genet*, 45:105–17, 2011.

9. H. R. Bode. The head organizer in Hydra. *Int. J. Dev. Biol.*, 56(6-8):473–8, 2012.

10. A. Böttger and M. Hassel. Hydra, a model system to trace the emergence of boundaries in developing eumetazoans. *Int. J. Dev. Biol.*, 56:583–91, 2012.

11. E. Braun and K. Keren. Hydra regeneration: Closing the loop with mechanical processes in morphogenesis. *BioEssays*, 40:1700204, 2018.

12. E. Braun and H. Ori. Electric-induced reversal of morphogenesis in hydra regeneration. *Bioph. J.*, 117(8):1514–1523, 2019.

13. F. Brinkmann, M. Mercker, T. Richter, and A. Marciniak-Czochra. Post-Turing tissue pattern formation: Advent of mechanochemistry. *PLoS Comput. Biol.*, 14:e1006259, July 2018.

14. M. Broun and H. R. Bode. Characterization of the head organizer in Hydra. *Development*, 129(4):875–84, Feb 2002.

15. M. Broun, L. Gee, B. Reinhardt, and H. R. Bode. Formation of the head organizer in Hydra involves the canonical Wnt pathway. *Development*, 132(12):2907–16, Jun 2005.

16. E. N. Browne. The production of new hydranths in Hydra by the insertion of small grafts. *J. Exp. Zool.*, 7(1):1–23, 1909.

17. W. Driever and C. Nüsslein-Volhard. A gradient of bicoid protein in drosophila embryos. *Cell*, 54(1):83–93, 1988.

18. J. Ferenc, P. Papasaikas, J. Ferralli, Y. Nakamura, S. Smallwood, and C. D. Tsiairis. Wnt3 expression as a readout of tissue stretching during Hydra regeneration. *bioRxiv*, doi:https://doi.org/10.1101/2020.12.22.423911, 2020.

19. A. C. Fröbius, G. Genikhovich, U. Kürn, F. Anton-Erxleben, and T. C. G. Bosch. Expression of developmental genes during early embryogenesis of Hydra. *Dev. Genes Evol.*, 213:445–55, Sept. 2003.

20. B. Galliot. Hydra, a fruitful model system for 270 years. *Int. J. Dev. Biol.*, 56(6-8):411–23, 2012.

21. B. Galliot and V. Schmid. Cnidarians as a model system for understanding evolution and regeneration. *Int. J. Dev. Biol.*, 46:39–48, Jan. 2002.

22. A. Gamba, M. Nicodemi, J. Soriano, and A. Ott. Critical behavior and axis defining symmetry breaking in Hydra embryonic development. *Phys .Rev. Lett.*, 108(15):158103, Apr 2012.

23. L. Gee, J. Hartig, L. Law, J. Wittlieb, K. Khalturin, and T. Bosch. Beta-catenin plays a central role in setting up the head organiser in hydra. *Dev. Biol.*, 340:226–24, 2010.

24. G. Genikhovich, U. Kürn, G. Hemmrich, and T. C. G. Bosch. Discovery of genes expressed in hydra embryogenesis. *Dev. Biol.*, 289:466–81, Jan. 2006.

25. A. Gierer. The hydra model - a model for what? *Int. J. Dev. Biol.*, 56:437–45, 2012.

26. A. Gierer, S. Berking, H. Bode, C. David, K. Flick, G. Hansmann, H. Schaller, and E. Trenkner. Regeneration of hydra from reaggregated cells. *Nature New Biol.*, 239: 91:98–101, 1972.

27. A. Gierer and H. Meinhardt. A theory of biological pattern formation. *Kybernetik*, 12(1):30–9, 1972.

28. C. Grimmelikhuijzen and H. Schaller. Hydra as a model organism for the study of morphogenesis. *TIBS*, 4:265–7, 1979.

29. C. Guder, I. Philipp, T. Lengfeld, H. Watanabe, B. Hobmayer, and T. W. Holstein. The Wnt code: cnidarians signal the way. *Oncogene*, 25:7450–60, Dec. 2006.

30. C. Guder, S. Pinho, T. G. Nacak, H. A. Schmidt, B. Hobmayer, C. Niehrs, and T. W. Holstein. An ancient Wnt-dickkopf antagonism in Hydra. *Development*, 133:901–11, Mar. 2006.

31. S. Gufler, B. Artes, H. Bielen, I. Krainer, M.-K. Eder, J. Falschlunger, A. Bollmann, T. Ostermann, T. Valovka, M. Hartl, K. Bister, U. Technau, and B. Hobmayer. β-Catenin acts in a position-independent regeneration response in the simple eumetazoan Hydra. *Dev. Biol.*, 433:310–23, Jan. 2018.

32. S. Härting and A. Marciniak-Czochra. Spike patterns in a reactiondiffusion ode model with turing instability. *Mathematical Methods in the Applied Science*, 37(9):1377–1391, 2013.

33. W. Helfrich. Elastic properties of lipid bilayers: theory and possible experiments. *Z Naturforsch [C]*, 28:693–703, 1973.

34. T. W. Hiscock and S. G. Megason. Mathematically guided approaches to distinguish models of periodic patterning. *Development*, 142(3):409–19, Feb 2015.

35. B. Hobmayer, F. Rentzsch, K. Kuhn, C. M. Happel, C. C. von Laue, P. Snyder, U. Rothbächer, and T. W. Holstein. Wnt signalling molecules act in axis formation in the diploblastic metazoan *Hydra*. *Nature*, 407(6801):186–9, Sep 2000.

36. T. W. Holstein. The evolution of the Wnt pathway. *CSH Perspect. Biol.*, 4:a007922, July 2012.

37. T. W. Holstein, E. Hobmayer, and U. Technau. Cnidarians: an evolutionarily conserved model system for regeneration? *Dev. Dyn.*, 226:257–67, Feb. 2003.

38. S. Kakugawa, P. F. Langton, M. Zebisch, S. Howell, T.-H. Chang, Y. Liu, T. Feizi, G. Bineva, N. O'Reilly, A. P. Snijders, E. Y. Jones, and J.-P. Vincent. Notum deacylates wnt proteins to suppress signalling activity. *Nature*, 519:187–192, 2015.

39. S. Kakugawa, P. F. Langton, M. Zebisch, S. Howell, T.-H. Chang, Y. Liu, T. Feizi, G. Bineva, N. O'Reilly, A. P. Snijders, E. Y. Jones, and J.-P. Vincent. Notum deacylates Wnt proteins to suppress signalling activity. *Nature*, 519(7542):187–192, 2015.

40. T. Käsbauer, P. Towb, O. Alexandrova, C. N. David, E. Dall'armi, A. Staudigl, B. Stiening, and A. Böttger. The Notch signaling pathway in the cnidarian Hydra. *Dev. Biol.*, 303:376–90, Mar. 2007.

41. Y. Komiya and R. Habas. Wnt signal transduction pathways. *Organogenesis*, 4:68–75, Apr. 2008.

42. L. Leclere, R. R. Copley, T. Momose, and E. Houliston. Hydrozoan insights in animal development and evolution. *Curr. Opin. Genet. Dev.*, 39:157–67, Aug. 2016.

43. T. Lengfeld, H. Watanabe, O. Simakov, D. Lindgens, L. Gee, L. Law, H. A. Schmidt, S. Ozbek, H. Bode, and T. W. Holstein. Multiple Wnts are involved in Hydra organizer formation and regeneration. *Dev. Biol.*, 330(1):186–99, Jun 2009.

44. A. Livshits, L. Shani-Zerbib, Y. Maroudas-Sacks, E. Braun, and K. Keren. Structural inheritance of the actin cytoskeletal organization determines the body axis in regenerating Hydra. *Cell Rep.*, 18:1410–21, 2017.

45. M. Lommel, J. Strompen, A. L. Hellewell, G. P. Balasubramanian, E. D. Christofidou, A. R. Thomson, A. L. Boyle, D. N. Woolfson, K. Puglisi, M. Hartl, T. W. Holstein, J. C. Adams, and S. Özbek. Hydra mesoglea proteome identifies thrombospondin as a conserved component active in head organizer restriction. *Sci. Rep.*, 8:11753, Aug. 2018.

46. H. K. MacWilliams. Numerical simulations of hydra head regeneration using a proportion-regulating version of the Gierer-Meinhardt model. *J. Theor. Biol.*, 99(4):681–703, 1982.

47. H. K. MacWilliams. Hydra transplantation phenomena and the mechanism of hydra head regeneration. I. Properties of the head inhibition. *Dev. Biol.*, 96:217–38, Mar. 1983.

48. H. K. MacWilliams. Hydra transplantation phenomena and the mechanism of hydra head regeneration. II. Properties of the head activation. *Dev. Biol.*, 96:239–57, Mar. 1983.

49. A. Marciniak-Czochra. Receptor-based models with hysteresis for pattern formation in hydra. *Math. Biosci.*, 199:97–119, 2006.

50. V. J. Martin, C. L. Littlefield, W. E. Archer, and H. R. Bode. Embryogenesis in hydra. *Biol. Bull.*, 192:345–63, June 1997.

51. H. Meinhardt. A model for pattern formation of hypostome, tentacles, and foot in hydra: how to form structures close to each other, how to form them at a distance. *Dev. Biol.*, 157(2):321–33, 1993.

52. H. Meinhardt. Modeling pattern formation in hydra: A route to understanding essential steps in development. *Int. J. Dev. Biol.*, 56(6-8):447–62, 2012.

53. H. Meinhardt. Turing's theory of morphogenesis of 1952 and the subsequent discovery of the crucial role of local self-enhancement and long-range inhibition. *Interface Focus*, 2:407–16, 2012.

54. H. Meinhardt and A. Gierer. Pattern formation by local self-activation and lateral inhibition. *Bioessays*, 22:753–60, 2000.

55. M. Mercker, F. Brinkmann, A. Marciniak-Czochra, and T. Richter. Beyond Turing: mechanochemical pattern formation in biological tissues. *Biol. Direct*, 11(22):1–15, May 2016.

56. M. Mercker, D. Hartmann, and A. Marciniak-Czochra. A mechanochemical model for embryonic pattern formation: coupling tissue mechanics and morphogen expression. *PLoS One*, 8(12):e82617, 2013.

57. M. Mercker, T. Holstein, S. Özbek, A. Tursch, and A. Marciniak-Czochra. How dickkopf molecules and wnt/β-catenin interplay to self-organise the *Hydra* body axis. *BioRxiv*, 2021.

58. M. Mercker, A. Köthe, and A. Marciniak-Czochra. Mechanochemical symmetry breaking in Hydra aggregates. *Biophys. J.*, 108(9):2396–407, May 2015.

59. M. Mercker, A. Marciniak-Czochra, T. Richter, and D. Hartmann. Modeling and computing of deformation dynamics of inhomogeneous biological surfaces. *SIAM Journal on Applied Mathematics*, 73(5):1768–1792, 2013.

60. W. A. Müller. Pattern control in Hydra: basic experiments and concepts. In H. Othmner, P. Maini, and J. Murray, editors, *Experimental and Theoretical Advances in Biological Pattern Formation*, pages 237–253. Boston: Springer, 1993.

61. S. Münder, S. Tischer, M. Grundhuber, N. Büchels, N. Bruckmeier, S. Eckert, C. A. Seefeldt, A. Prexl, T. Käsbauer, and A. Böttger. Notch-signalling is required for head regeneration and tentacle patterning in Hydra. *Dev. Biol.*, 383(1):146–57, Nov 2013.

62. Y. Nakamura, C. D. Tsiairis, S. Özbek, and T. W. Holstein. Autoregulatory and repressive inputs localize Hydra Wnt3 to the head organizer. *Proc. Natl. Acad. Sci. U S A*, 108(22):9137–42, May 2011.

63. K. Noda. Reconstitution of dissociated cells of Hydra. *Zoology*, 80:99–101, 1971.

64. J. J. Otto and R. D. Campbell. Budding in *Hydra attenuata*: bud stages and fate map. *J. Exp. Zool. A Ecol. Genet. Physiol.*, 200(3):417–28, 1977.

65. C. P. Petersen and P. W. Reddien. Wnt signaling and the polarity of the primary body axis. *Cell*, 139:1056–68, Dec. 2009.

66. I. Philipp, R. Aufschnaiter, S. Özbek, S. Pontasch, M. Jenewein, H. Watanabe, F. Rentzsch, T. W. Holstein, and B. Hobmayer. Wnt/beta-catenin and noncanonical Wnt signaling interact in tissue evagination in the simple eumetazoan Hydra. *Proc. Natl. Acad. Sci. U S A*, 106(11):4290–5, Mar 2009.

67. P. C. Reddy, A. Gungi, S. Ubhe, S. J. Pradhan, A. Kolte, and S. Galande. Molecular signature of an ancient organizer regulated by Wnt/β-catenin signalling during primary body axis patterning in Hydra. *Commun. Biol.*, 2(434), 2019.

68. B. Reinhardt, M. Broun, I. L. Blitz, and H. R. Bode. HyBMP5-8b, a BMP5-8 orthologue, acts during axial patterning and tentacle formation in hydra. *Dev. Biol.*, 267:43–59, Mar. 2004.

69. R. Rousset, J. A. Mack, K. A. Wharton, J. D. Axelrod, K. M. Cadigan, M. P. Fish, R. Nusse, and M. P. Scott. Naked cuticle targets dishevelled to antagonize Wnt signal transduction. *Genes Dev*, 15(6):658–671, 2001.

70. M. Sato, H. Tashiro, A. Oikawa, and Y. Sawada. Patterning in hydra cell aggregates without the sorting of cells from different axial origins. *Dev. Biol.*, 151:111–6, May 1992.

71. N. S. Scholes, D. Schnoerr, M. Isalan, and M. P. Stumpf. A comprehensive network atlas reveals that turing patterns are common but not robust. *Cell Sys.*, 9(3):243–57, 2019.

72. F. Schweisguth and F. Corson. Self-organization in pattern formation. *Dev. Cell*, 49:659–77, June 2019.

73. H. Shimizu. Transplantation analysis of developmental mechanisms in Hydra. *Int. J. Dev. Biol.*, 56(6-7-8):463–72, 2012.

74. K. M. Smith, L. Gee, and H. R. Bode. HyAlx, an aristaless-related gene, is involved in tentacle formation in hydra. *Development*, 127(22):4743–52, 2000.

75. J. Soriano, C. Colombo, and A. Ott. Hydra molecular network reaches criticality at the symmetry-breaking axis-defining moment. *Phys Rev Lett*, 97(25):258102, Dec 2006.

76. J. Soriano, S. Rüdiger, P. Pullarkat, and A. Ott. Mechanogenetic coupling of Hydra symmetry breaking and driven Turing instability model. *Biophys. J.*, 96(4):1649–60, Feb 2009.

77. R. E. Steele. Trembley's polyps go transgenic. *Proc. Natl. Acad. Sci. U S A*, 103:6415–6, Apr. 2006.

78. U. Technau, C. Cramer von Laue, F. Rentzsch, S. Luft, B. Hobmayer, H. R. Bode, and T. W. Holstein. Parameters of self-organization in Hydra aggregates. *Proc. Natl. Acad. Sci. U S A*, 97:12127–31, Oct. 2000.

79. U. Technau and T. W. Holstein. Cell sorting during the regeneration of Hydra from reaggregated cells. *Dev. Biol.*, 151(1):117–27, 1992.

80. U. Technau and T. W. Holstein. Head formation in Hydra is different at apical and basal levels. *Development*, 121(5):1273–82, 1995.

81. S. Tomczyk, K. Fischer, S. Austad, and B. Galliot. Hydra, a powerful model for aging studies. *Invertebrate Reproduction and Development*, 59:11–16, 2005.

82. A. Trembley. *Mémoires pour servir à l'histoire d'un genre de polypes d'eau douce, à bras en forme de cornes*, volume 1. Chez Jean & Herman Verbeek, 1744.

83. V. Trivedi, T. Fulton, A. Attardi, K. Anlas, C. Dingare, A. Martinez-Arias, and B. Steventon. Self-organised symmetry breaking in zebrafish reveals feedback from morphogenesis to pattern formation. *BioRxiv*, page 769257, 2019.

84. A. M. Turing. The chemical basis of morphogenesis. *Phil. Trans. R. Soc. Lond. B*, 237:37–72, 1953.

85. D. A. Turner, P. Baillie-Johnson, and A. Martinez Arias. Organoids and the genetically encoded self-assembly of embryonic stem cells. *BioEssays*, 38:181–91, Feb. 2016.

86. D. A. Turner, M. Girgin, L. Alonso-Crisostomo, V. Trivedi, P. Baillie-Johnson, C. R. Glodowski, P. C. Hayward, J. Collignon, C. Gustavsen, P. Serup, et al. Anteroposterior polarity and elongation in the absence of extra-embryonic tissues and of spatially localised signalling in gastruloids: mammalian embryonic organoids. *Development*, 144(21):3894–3906, 2017.

87. A. Tursch, N. B. M. Mercker, J. Schlüter, M. Lommel, A. Marciniak-Czochra, S. Özbek, and T. W. Holstein. Injury-induced MAPK activation triggers body axis formation in Hydra by default Wnt signaling. *Proc Natl Acad Sci U S A*, 119(35):doi: 10.1073/pnas.2204122119., 2022.

88. M. Veschgini, F. Gebert, N. Khangai, H. Ito, R. Suzuki, T. Holstein, Y. Mae, T. Arai, and M. Tanaka. Tracking mechanical and morphological dynamics of regenerating Hydra tissue fragments using a two fingered micro-robotic hand. *Appl. Phys. Lett.*, 108(10):103702, 2016.

89. M. Veschgini, H. O. Petersen, W. Abuillan, F. F. Rossetti, S. Özbek, M. Burghammer, T. W. Holstein, and M. Tanaka. Spatio-temporal elasticity patterns in extracellular matrix during hydra morphogenesis. *bioRxiv*, doi:https://doi.org/10.1101/214718, 2017.

90. M. C. Vogg, L. Beccari, L. Iglesias Oll[U+FFFD]. Rampon, S. Vriz, C. Perruchoud, Y. Wenger, and B. Galliot. An evolutionarily-conserved Wnt3/β-catenin/Sp5 feedback loop restricts head organizer activity in Hydra. *Nat. Commun.*, 10:312, Jan. 2019.

91. M. C. Vogg, B. Galliot, and C. D. Tsiairis. Model systems for regeneration: Hydra. *Development*, 146:https://doi.org/10.1242/dev.177212, Nov. 2019.

92. A. Wagner. Distributed robustness versus redundancy as causes of mutational robustness. *Bioessays*, 27(2):176–88, 2005.

93. H. Watanabe, H. A. Schmidt, A. Kuhn, S. K. Höger, Y. Kocagöz, N. Laumann-Lipp, S. Özbek, and T. W. Holstein. Nodal signalling determines biradial asymmetry in hydra. *Nature*, 515:112–5, Nov. 2014.

94. S. Werner, H. T.-K. Vu, and J. C. Rink. Self-organization in development, regeneration and organoids. *Curr. Opin. Cell Biol.*, 44:102–9, 2017.

95. K. A. Wharton, G. Zimmermann, R. Rousset, and M. P. Scott. Vertebrate proteins related to drosophila naked cuticle bind dishevelled and antagonize wnt signaling. *Dev Biol.*, 234(1):93–106, 2001.

96. L. Wolpert. Positional information and pattern formation. *Curr. Top. Dev. Biol.*, 6:183–224, 1971.

97. T. Yao. Studies on the organizer problem in Pelmatohydra oligactis: I. the induction potency of the implants and the nature of the induced hydranth. *J. Exp. Biol.*, 21(3-4):147–50, 1945.

98. X. Zhang, J. G. Abreu, C. Yokota, B. T. MacDonald, S. Singh, K. L. A. Coburn, S.-M. Cheong, M. M. Zhang, Q.-Z. Ye, H. C. Hang, H. Steen, and X. He. Tiki1 is required for head formation via Wnt cleavage-oxidation and inactivation. *Cell*, 149(7):165–177, 2012.

99. B. Ziegler, I. Yiallouros, B. Trageser, S. Kumar, M. Mercker, S. Kling, M. Fath, U. Warnken, M. Schnölzer, T. W. Holstein, M. Hartl, A. Marciniak-Czochra, J. Stetefeld, W. Stöcker, and S. Özbek. A Wnt-specific astacin proteinase controls head formation in Hydra. *biorxiv.org*, 2020.